Experimental Thermal and Fluid Science 33 (2009) 460–471

Contents lists available at ScienceDirect

Experimental Thermal and Fluid Science

journal homepage: www.elsevier.com/locate/etfs

The effects of freestream turbulence on the drag coefficient of a sphere

Niloofar Moradian [a], David S.-K. Ting [a,*], Shaohong Cheng [b]

[a] Mechanical, Automotive and Materials Engineering, University of Windsor, Windsor, Ontario, Canada N9B 3P4
[b] Civil and Environmental Engineering, University of Windsor, Windsor, Ontario, Canada N9B 3P4

ARTICLE INFO

Article history:
Received 20 May 2008
Received in revised form 30 October 2008
Accepted 3 November 2008

Keywords:
Sphere
Orifice perforated plate
Reynolds number
Drag
Turbulence intensity
Integral length scale

ABSTRACT

The effects of freestream turbulence intensity and integral length scale as freestream turbulent parameters on the drag coefficient of a sphere were experimentally investigated in a closed circuit wind tunnel. The Reynolds number, $Re = Ud/\nu$, was varied from 2.2×10^4 to 8×10^4 by using spheres with diameter d of 20, 51 and 102 mm in addition to altering the freestream velocity, U. The freestream turbulence intensity Tu and flow integral length scale Λ were manipulated by the utilization of orifice perforated plates. The proper combination of orifice perforated plate hole diameter, sphere size, and sphere location along the center line of the wind tunnel enabled the independent alterations of turbulence intensity and relative integral length scale (Λ/d) from 1.8% to 10.7% and from 0.1 to 2.6, respectively, at each studied Reynolds number. Results show that over the range of conditions studied, the drag always decreases with increasing Tu and, the critical Reynolds number at which the drag coefficient is dramatically reduced is decreased by increasing Tu. Most interestingly, the drag at any particular Re and Tu may be significantly lowered by reducing Λ/d; this is particularly the case at high Re and Tu.

1. Introduction

Sphere in turbulent freestream is a common phenomenon in our everyday life. In many engineering problems such as the flight of a weather balloon, the dispersion of aerosol sprays, rocket system, and the course of pollutants in the air and water, knowledge of parameters such as aerodynamic forces of spherical bodies in the presence of turbulent flow is often required. Sphere aerodynamics is also very important in sports such as golf, baseball and tennis.

The main characteristic of flow around a sphere is the existence of turbulent wake with recirculation [1], which has a dominant effect on the drag and lift of the sphere. The extent of this region depends on the size of the body, the velocity and viscosity of the fluid, which are cumulatively expressed as the Reynolds number. Moreover, it is also influenced by a wide variety of flow disturbances, which may originate from different sources.

For $Re < 0.1$, the flow near the sphere is essentially symmetrical as shown in Fig. 1a, [2]. For $0.1 < Re < 24$, inertial effects increase in importance near the sphere and the streamline pattern is no longer symmetrical [3], as shown in Fig. 1b. It can be seen from the standard logarithmic $C_D - Re$ curve in Fig. 2 [4,5] that in this range of very low Reynolds numbers, the drag coefficient of a sphere decreases logarithmically with increasing Reynolds number. At $Re \approx 24$, a small closed region of separated flow downstream of the rear stagnation point appears [6]. As the Reynolds number increases, a vortex recirculation grows within the separation bubble and its stability decreases; see Fig. 1c. For $Re < 100$, the sphere drag coefficient C_D varies as a function of $U^{-1/2}$, where U is the mean flow velocity [7]. At $Re \approx 130$, the downstream part of the separated region begins to oscillate [6]. This oscillation becomes stronger as Re increases up to about 210, but the laminar wake downstream of the wake stagnation point remains stable. For $210 < Re < 270$, an asymmetric separation bubble with a laminar wake has been observed [8]. Discrete vortex loops are shed periodically for $290 < Re < 700$ [9]. An increase in the level of freestream turbulence can cause the occurrence of vortex shedding at values as low as 150 [9]. The resultant shape of the vortex structure in the wake of the sphere is shown in Fig. 1d. As may be inferred from the figure, horse-shoe shaped vortex loops are formed [10–12]. These loops are rapidly detached from the near-wake region and form a series of vortices that are shed periodically into the far wake. As shown in Fig. 2, the logarithmic $C_D - Re$ curve is roughly linear in this range. But, for $Re > 700$, the logarithmic scale trend of $C_D - Re$ curve is no longer linear. However, unlike the drag coefficient for $Re < 100$, no special relation was found between the drag coefficient and the Reynolds number within the range of $100 < Re < 1000$ [7]. For $10^3 < Re < 3 \times 10^5$, the vortex shedding becomes nearly a continuous process. The wake structure in this flow regime is depicted in Fig. 1e. Fig. 2 shows that the value of C_D virtually remains constant in this regime. Lemmin et al. [7] found that when $Re > 2000$, C_D reaches a value of 0.39 and for

* Corresponding author. Tel.: +1 5192533000/2599; fax: +1 5199737007.
E-mail addresses: moradia@uwindsor.ca (N. Moradian), dting@uwindsor.ca (D.S.-K. Ting), shaohong@uwindsor.ca (S. Cheng).

0894-1777/$ - see front matter © 2008 Elsevier Inc. All rights reserved.
doi:10.1016/j.expthermflusci.2008.11.001

Nomenclature

C_D	drag coefficient
D	diameter of holes of the orifice perforated plates (m)
d	diameter of spheres (m)
F_{Bottom}	tensile force in a bottom string (N)
F_{D_Bottom}	streamwise tensile component in a bottom string (N)
F_D	drag force (N)
F_{D_Top}	streamwise tensile component in a top string (N)
F_{top}	tensile force in a top string (N)
N	sampling number
Re	Reynolds number, Ud/v
Re_{cr}	critical Reynolds number
Tu	turbulence intensity, $u_{rms}/\bar{U}$ (%)
U	mean flow velocity (m/s)
$\bar{U}$	time averaged velocity (m/s)
U_i	instantaneous velocity (m/s)
u	instantaneous fluctuating velocity (m/s)
u_{rms}	root mean square velocity (m/s)
Greek symbols	
Λ	integral length scale (m)
v	kinetic viscosity (m^2/s)
ς	autocorrelation factor
τ	time (s)
τ_Λ	integral time scale (s)
Δt	time interval between consecutive samples (s)

$2000 < Re < 10{,}000$, the drag coefficient varies with U^2. Around $Re \approx 3 \times 10^5$, transition to turbulence occurs in the boundary layer and the value of C_D drops dramatically as shown in Fig. 2. This Reynolds number is defined as the critical Reynolds number Re_{cr}. In the presence of turbulent boundary layer, separation moves to the rear of the sphere, Fig. 1f.

Since most applications of sphere–fluid interaction occur in practice involves turbulent freestream, in order to advance our understanding of the aerodynamics of sphere, it is imperative to have a proper knowledge of the role of freestream turbulence. A priori to understanding the aerodynamics of a sphere in complex turbulent flow encountered in engineering practice is a good comprehension of smooth sphere aerodynamics in simple turbulent freestream. Most past wind tunnel studies on the influence of freestream turbulence on sphere drag have not been very careful in keeping the turbulence clean. More importantly, there has been almost no attempt in separating the effect of fluctuating intensity from that of the turbulent length scales.

The flow downstream of an orifice perforated plate provides clean, simple and quasi-homogeneous freestream turbulence [13,14]. Quasi-isotropic turbulence was previously observed by Liu et al. [14] in the same experimental system, downstream of the 37.5 mm orifice perforated plate at 10.5 m/s. The orifice perforated plate turbulence was found to be homogeneous over the cross section normal to the mean flow with Gaussian-like turbulence fluctuation. The isotropy of the turbulence field as portrayed by the streamwise/lateral turbulence intensity ratio was found to be approximately 1.1. They also found that the turbulence kinetic energy decays in a power law form,

$$\frac{u'^2}{U^2} = A\left(\frac{X}{M} - \frac{X_0}{M}\right)^{-n} \tag{1}$$

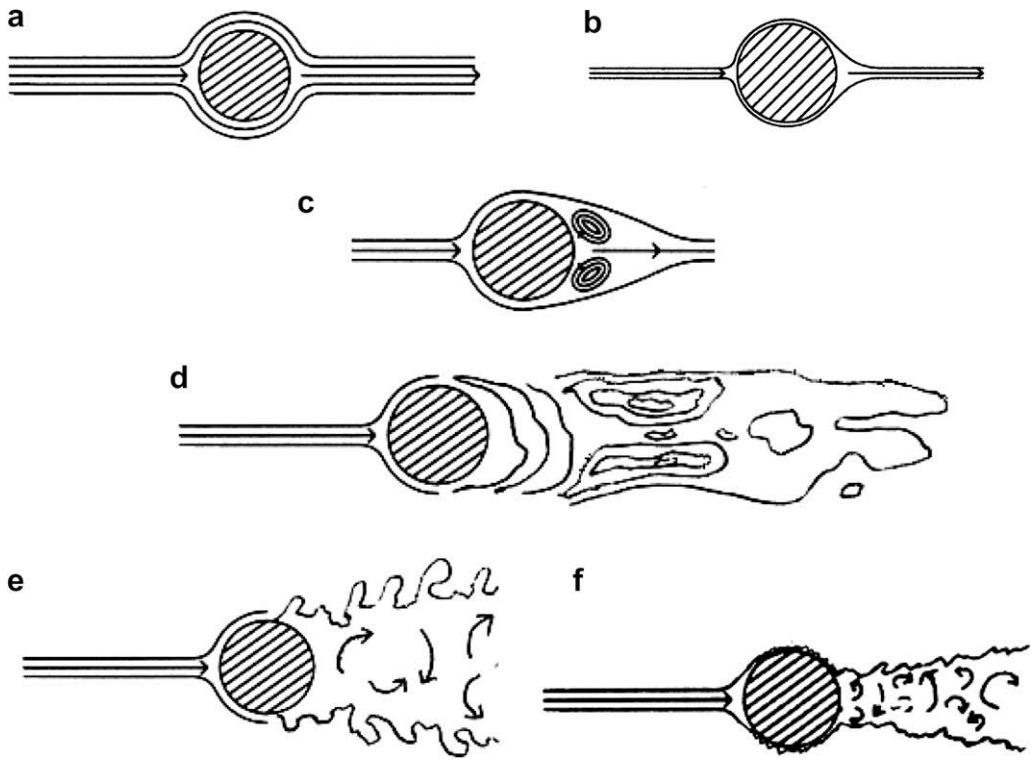

Fig. 1. Schematic of flow past a sphere at (a) $Re < 0.1$ (b) $0.1 < Re < 24$, (c) $24 < Re < 270$, (d) $270 < Re < 10^3$, (e) $10^3 < Re < 3 \times 10^5$ and (f) $Re > 3 \times 10^5$.

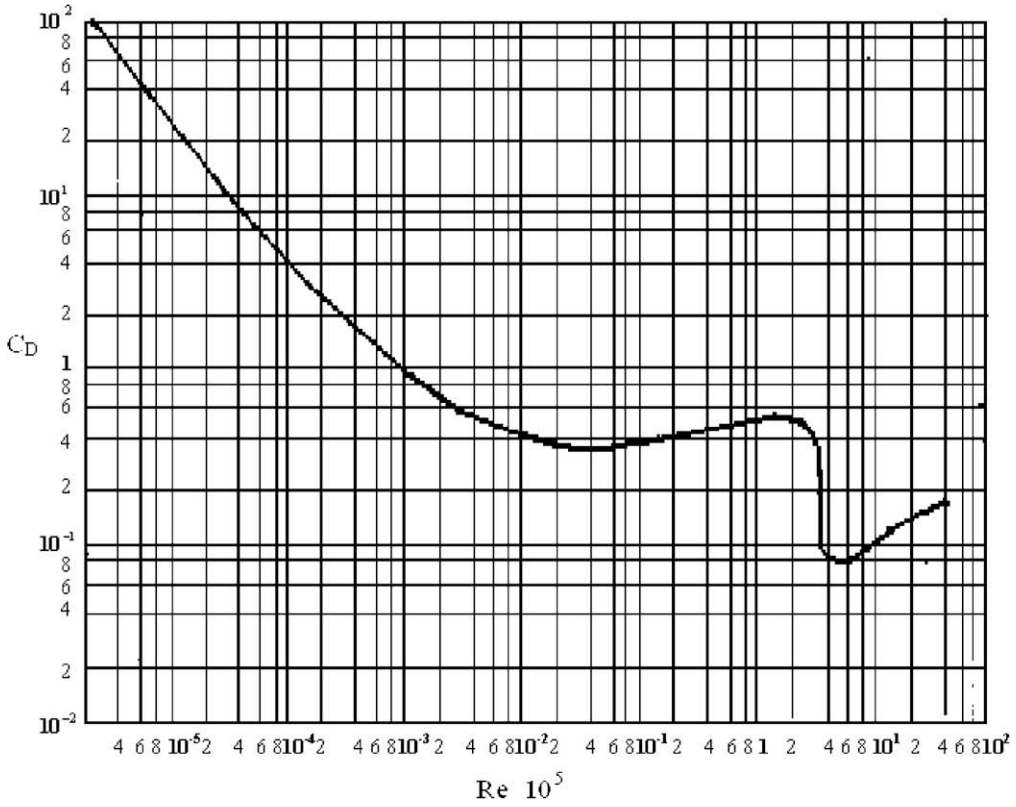

Fig. 2. Drag coefficient of the sphere as a function of Reynolds number [4,5].

where, X is streamwise coordinate, X_0 is the virtual origin, M is the size of the holes of the orifice perforated plate, A is the decay power law coefficient, and n is the decay power exponent. For the 37.5 mm orifice perforated plate considered, Liu et al. [14] obtained a value of 1.012 for the decay exponent, implying that the turbulence was in a self-preserving state. In this system, the integral length, Λ was found to be related to the turbulence decay coefficient, A in the power law decay of the turbulence kinetic energy in the form $\Lambda \propto A^{1/2}$. In other words, the higher the level of turbulence, the faster the rate of decay and, though to a lesser degree, the larger the integral length.

The literally omnipresent freestream turbulence may strongly influence the critical Reynolds number, Re_{cr}, at which the sphere boundary layer undergoes transition from laminar to turbulent. Furthermore, it can also affect the drag both beyond and below this transition point. Below the critical Reynolds number, it has been

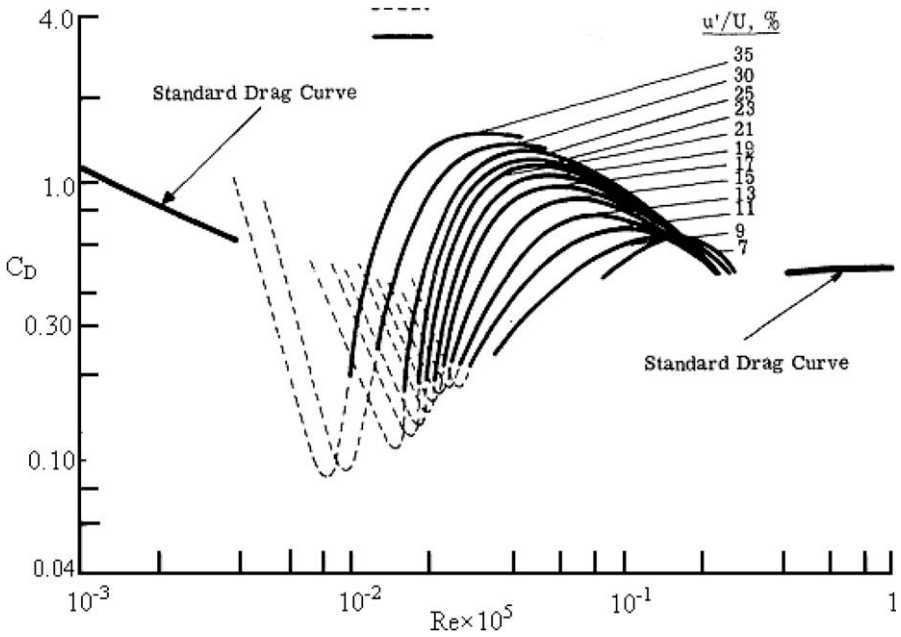

Fig. 3. Effect of turbulence on sphere drag [20].

observed that flow turbulence can cause a moderate increase in the drag coefficient as compared to that found in smooth flow [15]. By perturbing the flow, the separation point shifts downstream along the sphere surface, affecting the vorticity transfer and dissipation in the wake and hence, the form drag [16,17].

Dryden et al. [18] have documented that Re_{cr} decreases monotonically with the increase of turbulence intensity for levels up to 4.5%. The drag coefficient, after its sharp drop due to transition, rises steeply to a maximum and then drops off gradually [19,20], as portrayed in Fig. 3. The $C_D - Re$ curves corresponding to different turbulence intensity levels have similar shapes but the maximum C_D occurs at different Reynolds numbers [19,20]. The maximum C_D increases with the increase of turbulence intensity, while the Reynolds numbers at which the maximum C_D occurs decreases with increasing intensity [19,20]; see Fig. 3. After reaching their maxima, the $C_D - Re$ curves corresponding to different intensity levels tend to converge at higher Reynolds number [19,20]. It is worth noting that Refs. [19,20] have no mention of turbulence parameters other than turbulence intensity.

It is clear that freestream turbulence plays an important role in sphere aerodynamics. One key challenge to improving our understanding of the role of freestream turbulence on sphere aerodynamics is the multi-aspect of turbulence. The various turbulence characteristics and their effects on sphere aerodynamics are inter-dependent on each other. This study is limited to Re, Tu, Λ and/or Λ/d. In other words, the objective is to examine independently the influences of Reynolds number, turbulence intensity, freestream turbulence integral length scale and/or relative integral length scale on the drag of a sphere.

2. Experimental setup

The experiments were conducted in a closed-loop wind tunnel with a 4 m long test section. The test section is 0.75 m (width) × 0.75 m (height) at the inlet, and to accommodate for boundary layer built up, it expands to 0.765 m × 0.765 m at the end of the test section. The maximum attainable freestream velocity is around 20 m/s.

The turbulence was generated by placing one of the three orifice perforated plates at the inlet of the wind tunnel. These are 6 mm thick aluminum plates with holes of diameter D of 25, 37.5, and 50 mm, respectively, as shown in Fig. 4. The solidity ratio of the plates was fixed at 43%. To minimize the influence of the plate

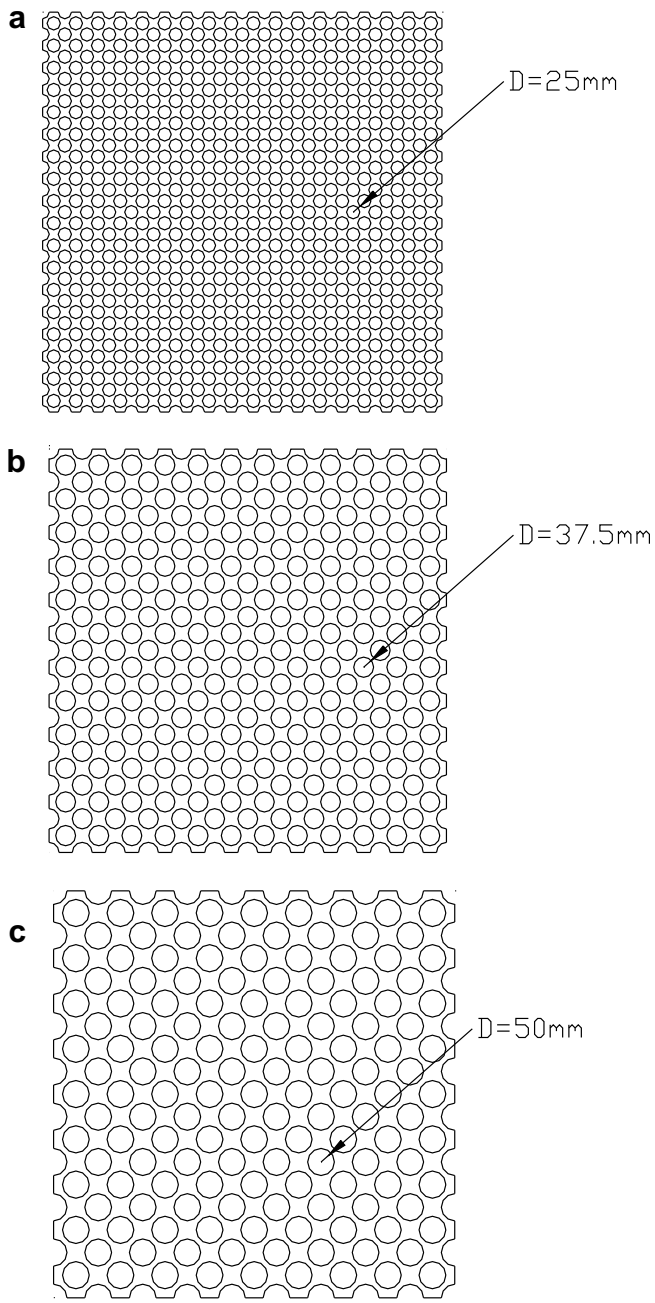

Fig. 4. Schematic of the orifice perforated plates (a) plate D-25, (b) plate D-37.5, and (c) plate D-50.

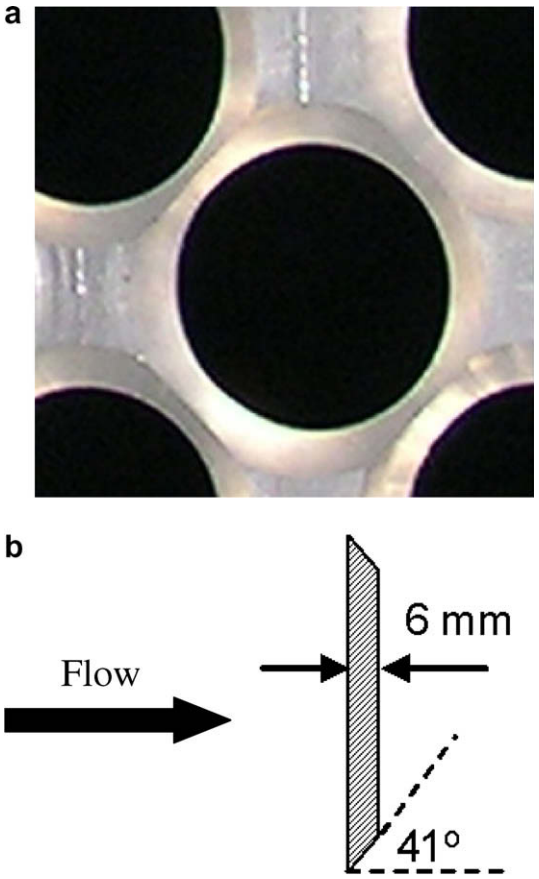

Fig. 5. The orifice perforated plate (a) looking upstream to the plate (b) cross section of the plate.

thickness on the turbulent flow field generated, each hole was machined into an orifice with a 41° angle as illustrated in Fig. 5. Studies by Liu and Ting [13,14] showed that an orifice perforated plate of 6 mm thickness, 41° orifice angle, and 43% solidity ratio was appropriate for generating quasi-isotropic turbulence.

The proper combination of orifice perforated plate hole diameter, sphere size, and sphere location enabled the independent alterations of turbulence intensity and relative integral length scale (Λ/d) from 1.8% to 10.7% and from 0.1 to 2.6, respectively, at each studied Reynolds number from 2.2×10^4 to 8×10^4.

To quantify the flow velocities and the associated turbulence parameters, a hot-wire system composed of a single normal wire of DISA type 55P11, a temperature probe, a Dantec Streamline 55C90 hot-wire anemometer (CTA) module, an A/D converter, a light-duty 2-D traversing system, and a computer were utilized. The traverse system was mounted at the desired location downstream of the orifice perforated plate for supporting the hot-wire probe and the temperature probe. It [13] has been shown that the turbulence generated by the orifice perforated plate remains non-isotropic until a distance of 10 D downstream of the plate. Thus, all hot-wire data in the current study were collected within a range of 10–50 D downstream of the orifice perforated plate, along the centerline of the test section. It was concluded from sensitivity analysis that a sampling frequency of 80 kHz and a minimum sample size of 7.6×10^6 were adequate in accurately deducing the flow parameters of interest. Thus, a sampling frequency of 80 kHz was used over a sampling time of 125 s, resulting in 10,000,000 samples at each measurement location. The collected data were low-passed at 30 kHz to avoid the aliasing problem before further analysis. A Pitot-static tube was employed when adjusting the power supply to the desirable wind speed. It was removed during hot-wire and drag measurement.

Three different sizes of spheres (d = 20, 51, 102 mm) were used in the present study to cover a Reynolds number range of 2.2×10^4 to 8×10^4, and to enable independent control of Λ/d from 0.1 to 2.6. All spheres were made of PVC and polished by light grade Scotch® hand-pad. The mean surface roughness was less than 1 μm, resulting in a relative roughness (mean surface roughness/sphere diameter) of no more than 0.5×10^{-4}. In other words, the spheres are mechanically smooth [21].

To minimize fixture effect on the sphere aerodynamics, the setup scheme by Bacon and Reid [22], of which strings were used to attach the sphere in the wind tunnel, was adopted in the present study. High strength polymer strings of 0.5 mm diameter (SF24G-150 model of the FUSION® brand) with maximum tensile load capacity of 10.9 kg were used to support the sphere. Each sphere was drilled with two threaded holes, both 9 mm in diameter and 20 mm in depth, for fastening the strings to the sphere via two screws. After the screws were tightly secured to the sphere, the holes were filled with Epoxy. A total of eight strings were used, four of which were fastened to the top hole and another four to the bottom one, as shown in Fig. 6. The other ends of the strings tied to the upper hole of the sphere were fastened firmly and laid symmetrically to the two side walls of the wind tunnel, each making an angle of 40.4° ± 0.3° with respect to the test section wall and 63.5° ± 0.3° to the streamwise direction of the wind tunnel. In the case of the bottom strings, the other ends were secured firmly to the floor of the wind tunnel making an angle of 45.2° ± 0.3° with

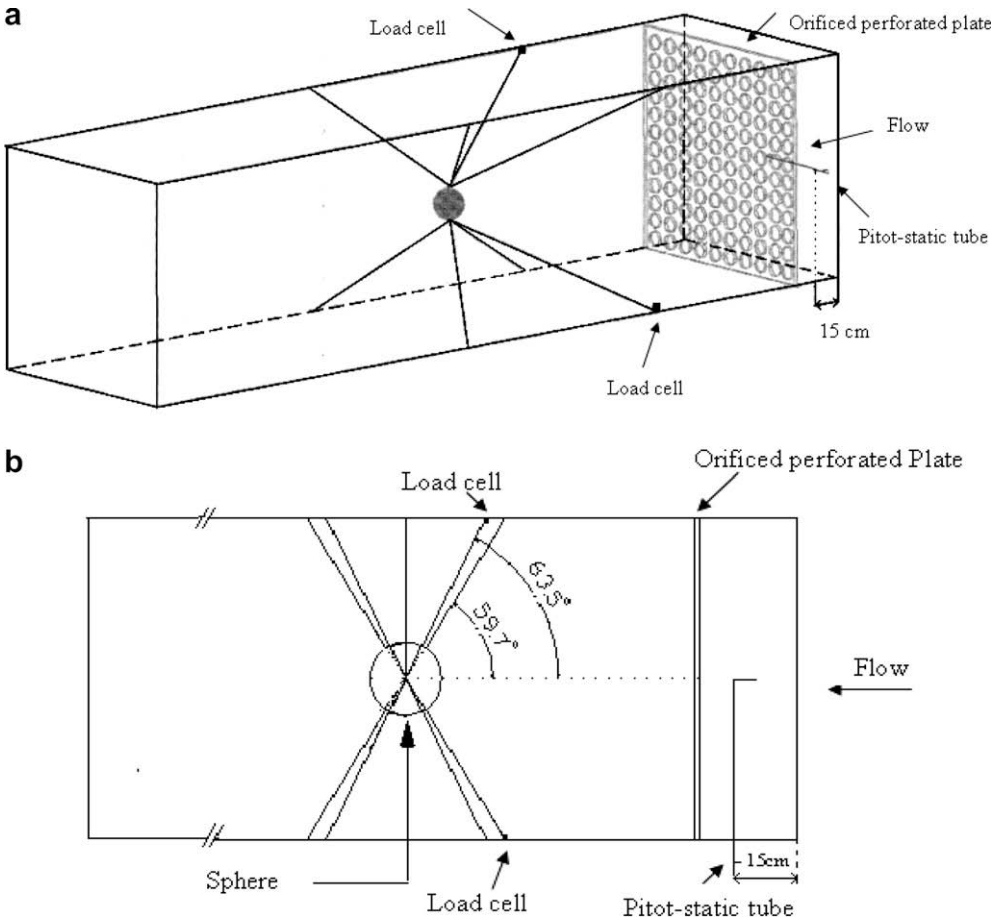

Fig. 6. Schematic of the load cell setup with the sphere supported by strings (a) perspective view (b) top view.

respect to the test section floor and 59.7° ± 0.3° with respect to the flow direction.

To measure the drag force of the sphere, a model ELG-V-1N-L03M ENTRAN load cell was utilized to quantify the tensile force in the strings. It has a full scale reading of 1 N, and an over-range limit of 10 N. It was connected to a model MROJHHSG Electro-Numerics Amplifier which provides a 10 V excitation to the load cell. For a supporting mechanism as portrayed in Fig. 6, when the sphere is subjected to the wind, only the four upstream strings, two at the top and two at the bottom, would resist the drag force on the sphere. In a typical testing case with specified wind velocity and turbulence level, the load cell was attached to one of the top upstream strings and one of the bottom upstream strings to quantify the tensile load within these two strings. Due to the symmetric layout of the strings, the drag of the sphere was therefore determined by the summation of the horizontal streamwise components of the tensile loads in these two strings multiplied by two. The following equations were used to calculate the drag force from the collected load cell data:

Streamwise tensile component in one top string:

$$F_{D\_Top} = \cos 63.5^{\circ} \times F_{top} \quad (2)$$

Streamwise tensile component in one bottom string:

$$F_{D\_Bottom} = \cos 59.7^{\circ} \times F_{bottom} \quad (3)$$

Total drag force on the sphere:

$$F_D = 2F_{D\_Top} + 2F_{D\_Bottom} \quad (4)$$

Three measures were taken during the test. First of all, all strings were tightened when fixing the sphere in the middle of the cross section. Secondly, the load-cell with the sphere supported by the strings were checked with a free-weight system in situ, pulling the sphere downstream in the absent of the wind. Over the range of load considered the deduction according to Eqs. (3) and (4) agreed quite well with this 'rough calibration'. Thirdly, prior to turning on the wind tunnel, the reading was zeroed. In other words, only the net load induced by the wind was measured. It is also worth mentioning that Bacon and Reid [22] have found that the string supporting system has negligible influence on the time-averaged drag measurement.

3. Hot-wire data analysis

The data collected by the hot-wire anemometer in terms of voltage values were converted to flow velocities using the calibration data. This procedure was done via a MATLAB program, which, for each of the input voltage value, gave the output as the instantaneous velocity. The time averaged velocity ($\bar{U}$) of the flow was simply the average of the whole sample acquired at any specific measurement location. By taking the difference between the time

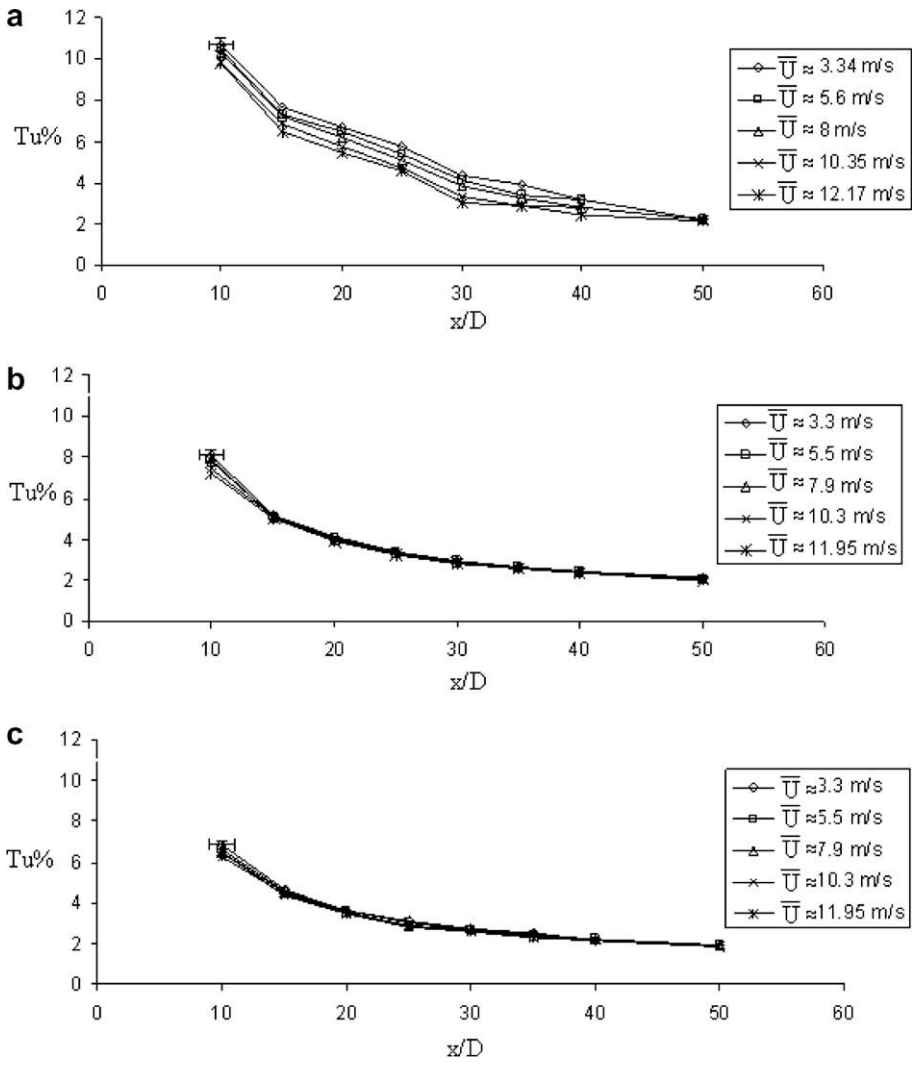

Fig. 7. Variation of turbulence intensity with respect to x/D (a) D = 25 mm (b) D = 37.5 mm (c) D = 50 mm.

averaged velocity and the instantaneous velocity (U_i), the instantaneous fluctuating velocity (u) was obtained. The root mean square velocity was deduced from:

$$u_{\mathrm{rms}} = \sqrt{\sum_{i=1}^{N} \frac{(U_i - \bar{U})^2}{N-1}} \tag{5}$$

where N is the sample size ($N = 10^7$). The turbulence intensity (Tu) was simply obtained from:

$$Tu = 100 \times \frac{u_{\mathrm{rms}}}{\bar{U}} \tag{6}$$

The integral time scale

$$\tau_{\Lambda} = \int_0^{\infty} \varsigma(\tau)\mathrm{d}\tau \tag{7}$$

was deduced via

$$\tau_{\Lambda} = \left(\sum_{i=1}^{N-1} \varsigma(i\Delta t)\right)\Delta t \tag{8}$$

where the autocorrelation factor (ς) for discrete samples was calculated from

$$\varsigma(m\Delta t) = \frac{\frac{1}{N-m}\sum_{i=1}^{N-m}(U_i U_{i+m})}{\frac{1}{N}\sum_i^N U_i^2} \tag{9}$$

where m varies from 0 to $N-1$.

Invoking the Taylor's frozen hypothesis [23], the integral time scale was then multiplied by the time averaged velocity at each location to obtain the corresponding integral length scale:

$$\Lambda = \bar{U} \cdot \tau_{\Lambda} \tag{10}$$

According to Batchelor [24], this hypothesis is valid for turbulence intensity up to 15%. The maximum turbulence intensity considered in this study was 10.7%; thus, the integral scale estimation is expected to be reliable.

4. Results and discussion

Within the limit posted by the three available orifice perforated plates, the range of freestream velocity the wind tunnel can

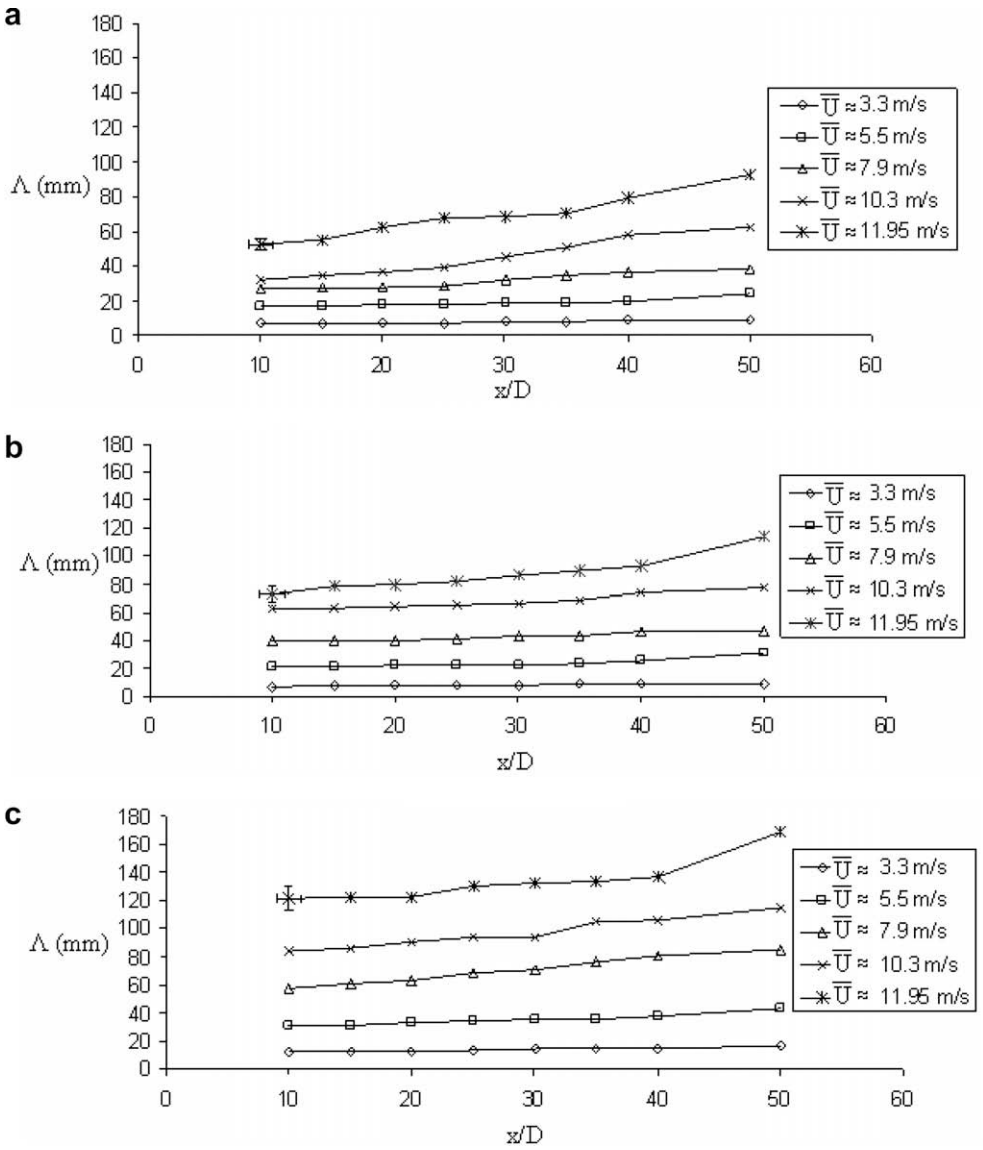

Fig. 8. Variation of integral length scale with respect to x/D (a) $D = 25$ mm (b) $D = 37.5$ mm (c) $D = 50$ mm.

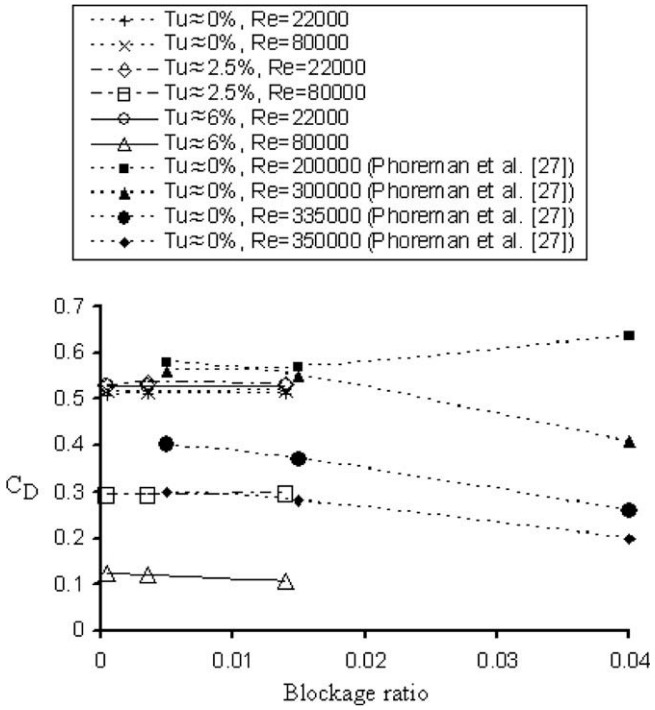

Fig. 9. Blockage effect on the drag coefficient of a sphere.

provide, and the length of the test section over which the turbulence is significant and quasi-isotropic, attempt was made to pinpoint conditions (plate, wind speed, distance downstream of the plate) which would provide at least three data points on the independent effects of *Tu*, *Re*, and Λ/d. Drag measurements were also taken in the absence of the orifice perforated plate, where the free-stream turbulence was less than 0.3%. These 'smooth flow' results are compared with those of the 'standard curve'.

The uncertainty in the hot-wire measurement came primarily from the calibration, that is, from the velocity measurement, the curve fitting and the digitization process. The uncertainty in using the Pitot-static tube to measure the nozzle air jet velocity was 2.1%. Curve fitting resulted in 0.5% uncertainty. The uncertainty in the digitization process for the 12 bits A/D with an input range set as 0–10V was $(0.5 \times 10)/2^{12} = 0.0012V$ [25]. Thus, the overall uncertainties in $\bar{U}$ and u_{rms} are around 2.2% and 3%, respectively. The corresponding uncertainties in turbulence intensity and integral length scale are 3.7% and 7.1%, respectively.

The uncertainty of the drag coefficient came primarily from four sources, i.e. the sphere diameter measurement, the velocity measurement, the air density estimation, and the load cell measurement. The diameter of the sphere was measured with a dial-caliper. The caliper has a resolution of 0.0254 mm and hence, an accuracy of ±0.0127 mm. In addition, repeated measurements showed a repeatability uncertainty of ±0.8 mm. Thus, the total uncertainty of sphere diameter was 0.31%. The uncertainty in the mean velocity measurement was 2.2% and that of the measured drag force was 10.4%. The uncertainty in the air density was negligible in comparison with others. The drag coefficient C_D was deduced from $C_D = F_D/[0.5\rho U^2(\pi d^2/4)]$, resulting in a maximum uncertainty of around 11%.

4.1. Orifice perforated plate turbulence

As mentioned in Section 1, the turbulence kinetic energy was found to decay in a power law form according to Eq. (1). For the 37.5 mm orifice perforated plate, an exponent of 1.012 was obtained by Liu et al. [14]; while the value varied from 1.02 to 1.09 in the current work, depending on the velocity, as shown in Fig. 7. Our measurements also agree favorably with the analytical prediction by Speziale and Bernard [26]; who showed that $n = 1$ is the asymptotic solution for completely self-preserving, isotropic turbulence.

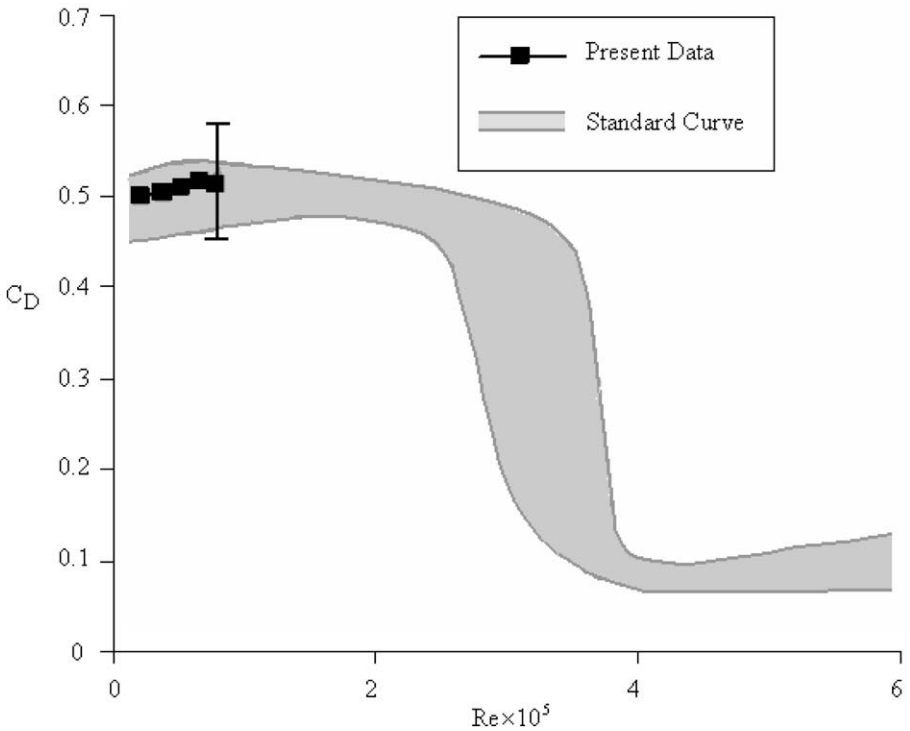

Fig. 10. Drag coefficient versus Reynolds number in the absence of orifice perforated plate.

Integral length scale is the coherent structure which represents the size of the energy containing eddies. For grid turbulence, the magnitude of integral length scale is largely dependent on the test apparatus, that is, the size of the holes and the spacing between them. Fig. 8 shows the variation of integral length scale downstream of the orifice perforated plate. These results are also consistent with earlier measurements obtained by Liu et al. [13,14].

4.2. Blockage effect on drag coefficient

Blockage is defined as the ratio between the cross-sectional area of a sphere and that of the wind tunnel test section. Phoreman et al. [27] investigated the effect of blockage on the measured drag in the 840 mm high and 1200 mm wide UC Davis Aeronautical wind tunnel where the background turbulence intensity was less than 0.1%. Blockage ratios of 0.6%, 1.5% and 3.9% were simulated using spheres of 87.5 mm, 137.5 mm and 225 mm diameters. Phoreman et al. found that the effect of blockage is negligible when the blockage ratio is less than 0.02. Beyond a blockage ratio of 0.02, the drag coefficient increases with increasing blockage for Reynolds number less than the critical value ($Re < Re_{cr} \approx 3 \times 10^5$); see Fig. 9. On the other hand, for $Re \geqslant Re_{cr}$, increasing blockage decreases the drag. The maximum blockage encountered in the present study is 0.015. In agreement with Phoreman et al. [27], this small amount of blockage does not have any detectable effect on C_D; see Fig. 9.

4.3. Drag of sphere under 'smooth flow' condition (Tu < 0.3%)

In the absence of the orifice perforated plate, the turbulence intensity Tu in the wind tunnel was measured to be less than 0.3%. Thus, the measured drag is expected to agree with the standard values in the literature. Fig. 10 portrays a comparison between the $C_D - Re$ relation achieved in this study and the standard curve, where the band of the standard curve is based on date from Schlichting [5], Lapple and Shepherd [28], Clift and Gauvin [29,30], and Achenbach [31]. The values of drag coefficient obtained in this study fall around the middle of the band of the standard curve.

4.4. Effect of integral length scale

Fig. 11 shows the impact of integral length scale Λ on the sphere drag while holding the turbulence intensity fixed. It can be seen that the drag coefficient increases (approaching the standard 'smooth flow' value) with the increase of integral length scale. For $Re < 5.3 \times 10^4$, this decrease of C_D with decreasing Λ is marginal. However, at higher Reynolds numbers, this C_D reduction

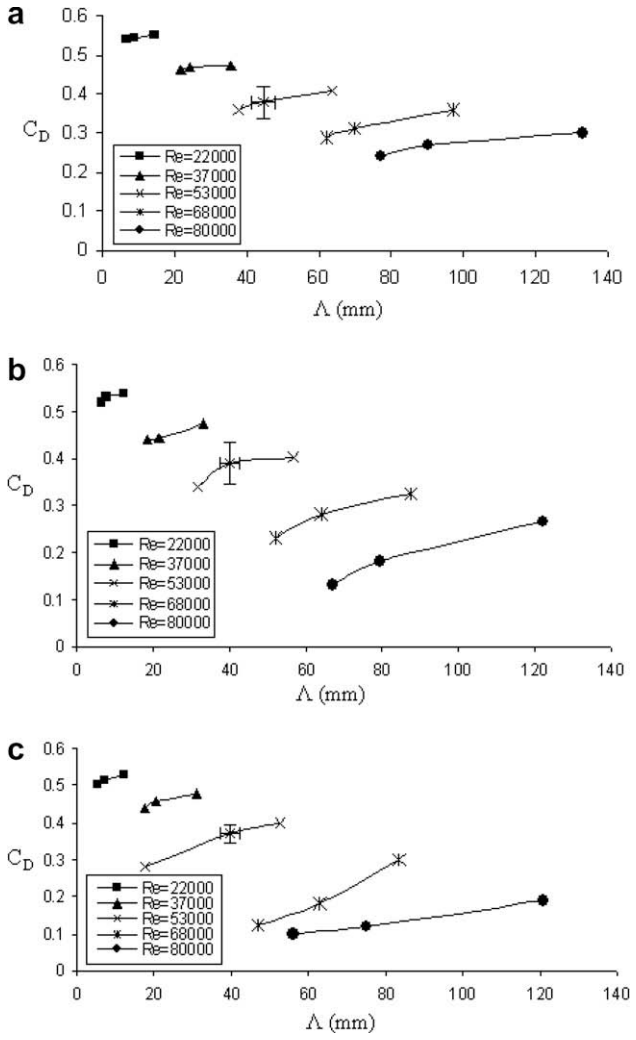

Fig. 11. Impact of integral length scale on sphere drag when (a) Tu = 2.5% (b) Tu = 4% (c) Tu = 6.3%.

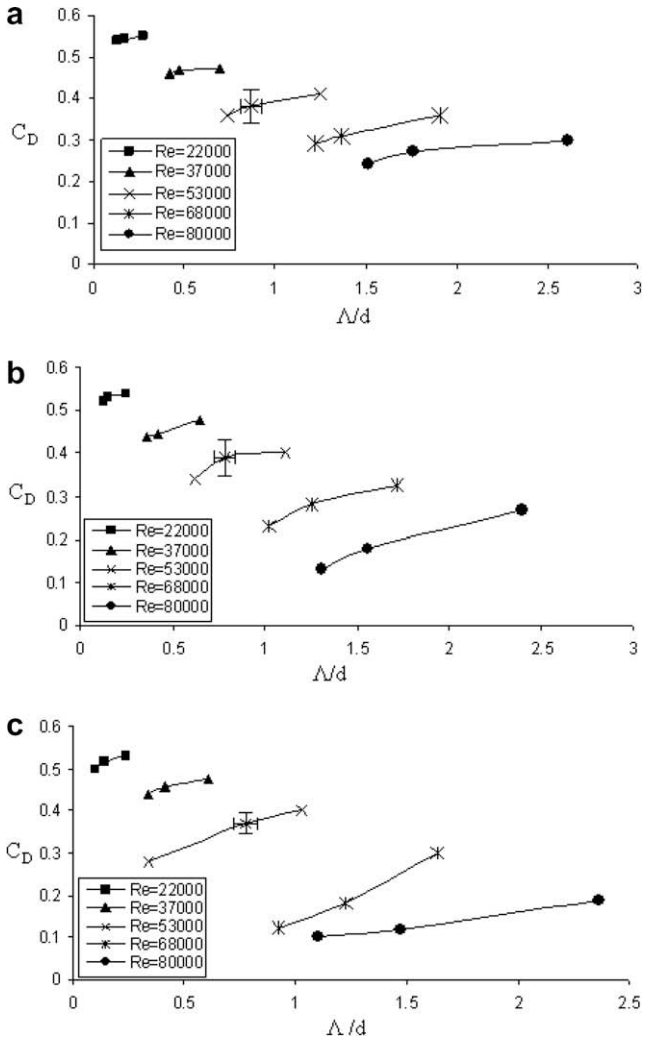

Fig. 12. Impact of relative integral length scale on sphere drag when (a) Tu = 2.5% (b) Tu = 4% (c) Tu = 6.3%.

effect becomes more significant. At $Re = 8 \times 10^4$, for example, when $Tu = 4\%$, the drag coefficient decreases by more than half, from 0.27 to 0.13 when the integral length scale is decreased from 122 to 67 mm.

The extent of C_D reduction with decreasing Λ is also dependent on the turbulence intensity; compare Fig. 11a–c. At $Tu = 2.5\%$, Fig. 11a, the drag is only slightly reduced with decreasing integral length. At $Tu = 4\%$, Λ effect on C_D is more visible, specially for $Re > 5.3 \times 10^4$; see Fig. 11b. In other words, the effect of integral length scale on C_D becomes progressively more significant with increasing turbulence intensity. Fig. 11c shows that the largest decrease in C_D with decreasing Λ occurs at $Re \approx 6.8 \times 10^4$; where C_D is reduced from 0.3 to 0.12 when decreasing Λ from 84 to 47 mm.

If critical Reynolds number is defined as the Reynolds number at which the drag coefficient drops to around 0.1 [4], then it can be seen, for example, that this occurs for $Re = 8 \times 10^4$, $Tu = 6.3\%$, and $\Lambda \approx 55$ mm as shown in Fig. 11c. Thus, under this set of physical combination, Re_{cr} is reduced from $Re_{cr} = 3.5 \times 10^5$ in the standard situation to approximately 8×10^4.

Besides Λ, the differences in the boundary layer thickness and wake size due to different sphere size may also affect C_D. To elim-

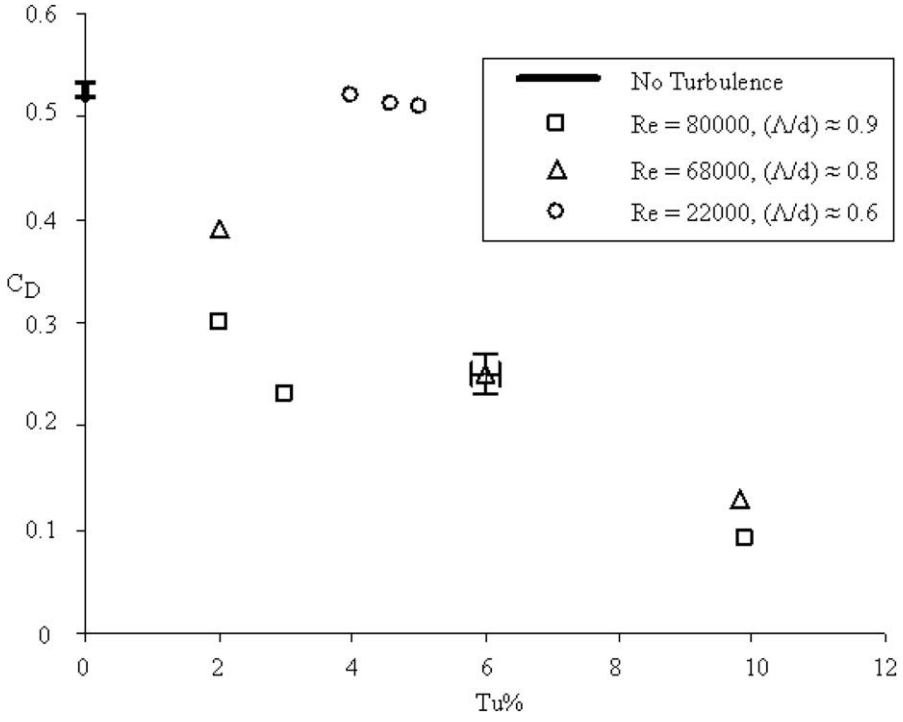

Fig. 13. Impact of turbulence intensity on sphere drag.

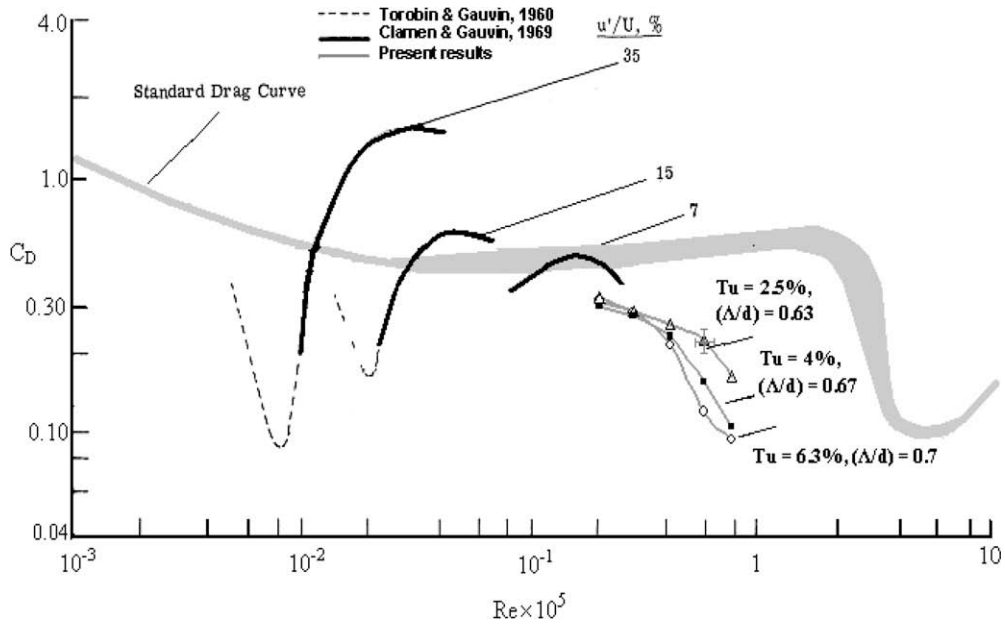

Fig. 14. Impact of Reynolds number on sphere drag and comparison of $C_D - Re$ results.

inate the effect of sphere size, a non-dimensional parameter, the relative integral length scale (Λ/d) is introduced.

Fig. 12 shows the impact of relative integral length scale on the sphere drag while holding the turbulence intensity fixed. As can be observed from the figure, the effect of relative integral length scale on drag coefficient is similar to that of the integral length scale.

4.5. Effect of turbulence intensity

At the critical Reynolds number $Re_{cr} = 3.5 \times 10^5$, the boundary layer changes from laminar to a turbulent one and consequently, the wake becomes narrower. This narrowing of wake has been observed to occur at $Re < 3.5 \times 10^5$ when the freestream turbulence is enhanced [1]. In other words, the critical Reynolds number can be significantly advanced by augmenting the flow stream turbulence, resulting in a significant drop in the drag coefficient at Reynolds number much lower than the standard critical value [32,33].

Fig. 13 shows the impact of turbulence intensity on the sphere drag while holding the relative integral length scale Λ/d fixed. The small extent on the *Y*-axis corresponds to the 'no turbulence' scenario obtained in the absence of an orifice perforated plate. At $Re \approx 2.2 \times 10^4$, increasing the turbulence intensity only leads to marginal decrease in the drag coefficient. A typical case with $(\Lambda/d) \approx 0.6 \sim 0.9$ is shown in Fig. 13; results at other (Λ/d) values show the same trend. At a higher Reynolds number of 6.8×0^4, the turbulence intensity is significantly more effective in reducing the drag. This is particularly true for $(\Lambda/d) \leqslant 1$; recall in Figs. 11 and 12 that increasing the relative integral length scale above unity decreases the turbulence intensity effectiveness in reducing the drag coefficient. Larger still is the effect of *Tu* in decreasing C_D at $Re \approx 8 \times 10^4$ as portrayed in Fig. 13; where the drag coefficient drops below 0.1 when the turbulence intensity is 10%, for the relative integral length scale around 0.9.

4.6. Effect of Reynolds number

Fig. 13 has indicated that the effectiveness of turbulence intensity in lowering C_D increases with Re. To illustrate this (better) from another angle, C_D is plotted against *Re* in Fig. 14. Fig. 14 portrays the $C_D - Re$ relationships with fixed (Λ/d) and *Tu*. The data obtained from the present study correspond to a relative integral length scale of 0.7 (roughly medium value over the $0.1 < (\Lambda/d) < 2.6$ range considered in this study) clearly depicts that the decrease in the drag coefficient, with increasing Reynolds number, becomes progressively more significant as the turbulence intensity is augmented.

4.7. Comparison with other studies

Also plotted in Fig. 14 are some relevant results scattered in the open literature. Fig. 14 shows the comparison between the standard ('smooth flow') curve [4], the results of Torobin and Gauvin [19], Clamen and Gauvin [20] and ours. It should be stressed again that neither Torobin and Gauvin nor Clamen and Gauvin have considered turbulent length scale in their studies. In other words, there is a hidden turbulence length scale effect among their curves of different turbulence intensities. After all, we would expect fluctuating eddies of the size of the boundary layer just before the separation point to be more effective in shifting the point at which separation occurs. Furthermore, the inherent three-dimensional nature of the flow around the sphere in the wake region may be influenced by integral scales of oncoming turbulence.

To put our results into perspective, the $(\Lambda/d) \approx 0.7$ case was chosen. Roughly speaking, our results fall within the general trend extrapolated from Clamen and Gauvin's $Tu = 7\%$ result. If this extrapolation is correct, Clamen and Gauvin's curve seems to suggest a pre-critical Reynolds number reduction in C_D. This pre-Re_{cr} reduction in C_D appears to occur along the 'saddle' of the $C_D - Re$ curve. Over the ranges of *Tu* and *Re* covered in this study, our results, however, do not hint towards any sinking of $C_D - Re$ saddle with increasing turbulence level.

5. Conclusion

The effects of Reynolds number, turbulence intensity and integral length scale on the drag coefficient of a sphere were experimentally investigated in a closed circuit wind tunnel. The Reynolds number, $Re = Ud/v$, was varied from 2.2×10^4 to 8×10^4. The proper combination of orifice perforated plate hole diameter, sphere size, and sphere location enabled the independent alterations of turbulence intensity and relative integral length scale (Λ/d) from 1.8% to 10.7% and from 0.1 to 2.6, respectively, at each studied Reynolds number.

Current results have confirmed that the drag coefficient is decreased with increasing turbulence intensity, and the value of Re_{cr} at which C_D drops below 0.1 can be advanced when the flow stream turbulence is significantly intense. More interestingly, the unique role of the relative integral length scale is revealed. The drag can be reduced significantly by decreasing the integral length. This is particularly true when the level of turbulence is high.

In practice there are many situations in which a spherical body is inserted into a conduit where turbulent fluid is being transported. To reduce losses (pumping power), the body may be sized based on the prevailing freestream integral length scale. When using a sphere for calibrating the flow quality of a wind tunnel, cares should be taken to avoid using a sphere which is of the size of (or slightly larger than) the integral scale.

Acknowledgments

The authors are grateful to Natural Sciences and Engineering Research Council of Canada (NSERC) for supporting this project. We are also very grateful to the diligent reviewers for their excellent comments.

References

[1] H. Tyagi, R. Liu, D.S.K. Ting, C.R. Johnston, Measurement of wake properties of a sphere in freestream turbulence, Experimental Thermal and Fluid Science 30 (2006) 587–604.
[2] H. Lamb, Hydrodynamics, sixth ed., Dover Publications, New York, 1945.
[3] V.G. Jenson, Viscous flow around a sphere at low Reynolds numbers (<40), Royal Society – Proceedings (London) (Ser. A) 249 (1959) 346–366.
[4] L.B. Torobin, W.H. Gauvin, Fundamental aspects of solids-gas flow. Part II: the sphere wake in steady laminar fluids, Canadian Journal of Chemical Engineering 37 (1959) 167–176.
[5] H. Schlichting, Boundary-Layer Theory, seventh ed., McGraw-Hill, New York, 1979.
[6] S. Taneda, Studies of wake vortices (III), experimental investigation of the wake behind a sphere at low Reynolds numbers, Report in Research Institute of Applied Mechanics of Japan 4 (1956) 99–105.
[7] U. Lemmin, M. Schurter, D.M. Imboden, Th. Joller, An instrument for measuring small currents in lakes, The American Society of Limnology and Oceanography (1985) 1116–1122.
[8] R.H. Margarvey, R.L. Bishop, Transition ranges for three-dimensional wakes, Canadian Journal of Physics 39 (1961) 1418–1422.
[9] K.R. Sivier, J.A. Nicholls, Subsonic Sphere Drag Measurements at Intermediate Reynolds Numbers, NASA Contractor Report No. 1392 (1969) 68.
[10] R.H. Magarvey, C.S. Maclatchy, Formation and structure of vortex rings, Canadian Journal of Physics 42 (1964) 678–683.
[11] E. Achenbach, Vortex shedding from spheres, Journal of Fluid Mechanics 62 (23, January) (1974) 209–221.
[12] D. Ormieres, M. Provansal, Transition to turbulence in the wake of a sphere, Physical Review Letters 83 (5, July) (1999) 80–83.
[13] R. Liu, D.S-K. Ting, Turbulent flow downstream of a perforated plate: sharp-edged orifice versus finite-thickness holes (n 8), Journal of Fluids Engineering 129 (September) (2007) 1164–1171.

[14] R. Liu, D.S.-K. Ting, M.D. Checkel, Constant Reynolds number turbulence downstream of an orificed, perforated plate, Experimental Thermal and Fluid Science 31 (2007) 897–908.
[15] N.A. Zarin, Measurement of and Turbulence Subsonic Sphere Non-continuum Effect on Drag, University of Michigan for Lewis Research Center, National Aeronautics and Space Administration, Washington, 1970.
[16] J.M. Kendall, The Periodic Wake of a Sphere, Propulsion Laboratory, California Institute Technology, Space Programs Summary No. 37-25, vol. 4, 1964, p. 251.
[17] H.F. Winny, The Vortex System Generated Behind a Sphere Moving Through a Viscous Fluid, Aeronautical Research Council R and M (No. 1531), 1932.
[18] H.L. Dryden, G.B. Schubauer, W.C. Mock, H.K., Measurements of Intensity and Scale of Wind Tunnel Turbulence and their Relation to the Critical Reynolds Number of Spheres, NACA Report No. 581, 1937.
[19] L.B. Torobin, W.H. Gauvin, Fundamental aspects of solids–gas flow. Part V: the effects of fluid turbulence on the particle drag coefficient, Canadian Journal of Chemical Engineering 38 (1960) 189–200.
[20] A. Clamen, W.H. Gauvin, Effects of turbulence on the drag coefficients of spheres in a supercritical flow regime, American Institute of Chemical Engineers (AIChE) Journal 15 (1969) 184–189.
[21] J. Westerman, E. Sharcos, Din 140: 1304 Standard, (1966), pp. 160–200.
[22] D.L. Bacon, E.G. Reid, The Resistance of Spheres in Wind Tunnels and in Air Report No. 185, National Advisory Committee for Aeronautics, United States National Advisory Committee for Aeronautics, (1924), p. 21.
[23] G.I. Taylor, The spectrum of turbulence, Proceeding of the Royal Society London (Ser. A164) (1938) 476–490.
[24] G.K. Batchelor, An Introduction to Fluid Dynamics, Cambridge University Press, Cambridge, 1967.
[25] Dantec Dynamics, Streamline_streamware Installation and Users Guide, Denmark, 2000.
[26] C.G. Speziale, P.S. Bernard, The energy decay in self-preserving isotropic turbulence revisited, Journal of Fluid Mechanics 241 (1992) 645–667.
[27] J. Phoreman, S. Saephan, J.C. Vander Kam, Determination of Turbulence Level in the UC Davis Aeronautical Wind Tunnel. http://windtunnel.engr.ucdavis.edu/research/spheres/sphereport.pdf. 2007 (accessed 15.12.07).
[28] C.E. Lapple, C.B. Shepherd, Flow pattern and pressure drop in cyclone dust collectors, Industrial and Engineering Chemistry 32 (1940) 1246–1248.
[29] R. Clift, W.H. Gauvin, The motion of particles in turbulent gas streams, in: Chemeca 70: A Conference Convened by the Australian National Committee of the Institution of Chemical Engineers and the Australian Academy of Science. Butterworths of Australia and the Institution of Chemical Engineers, Chatswood, Australia, 1970, pp. 14–28.
[30] R. Clift, W.H. Gauvin, Motion of entrained particles in gas streams, Canadian Journal of Chemical Engineering 49 (1971) 439–448.
[31] E. Achenbach, Experiments on the flow past spheres at very high Reynolds numbers, Journal Fluid Mechanics 54 (1972) 565.
[32] H.L. Dryden, G.B. Schubauer, W.C. Mock, H.K. Bkrambtad, Measurements of Intensity and Scale of Wind-tunnel Turbulence and their Relation to the Critical Reynolds number of spheres, National Advisory Committee for Aeronautics – Report No. 581, 1937, p. 32.
[33] D.L. Bacon, E.G. Reid, The Resistance of Spheres in Wind Tunnels and in Air, Report No. 185, NACA, United States National Advisory Committee for Aeronautics, 1924.